Stability of periodic traveling waves for the hydroelastic Whitham equation

Marcelo V. Flamarion [a] [iD],*, Jimmie Adriazola [b]

[a] *Departamento Ciencias—Sección Matemáticas, Pontificia Universidad Católica del Perú, Av. Universitaria 1801, San Miguel 15088, Lima, Peru*
[b] *School of Mathematical Sciences and Statistics, Arizona State University, United States of America*

ARTICLE INFO

ABSTRACT

In this work, we investigate the stability of hydroelastic periodic traveling waves within a Whitham-type equation framework. The Whitham equation is well known in the literature as a relatively simple model that nevertheless captures rich nonlinear phenomena such as short waves and breaking. Periodic traveling waves are computed numerically, and their stability is analyzed by evaluating the spectrum via the Fourier–Floquet–Hill method. We show that for small values of the flexural rigidity coefficient, small-amplitude periodic traveling waves are unstable; however, as the amplitude increases beyond a critical threshold, we first observe stabilization (not complete); subsequently, the spectrum bifurcates, and the traveling waves become increasingly unstable. In contrast, when the flexural rigidity coefficient is large, periodic traveling waves remain stable for all amplitudes. For moderate elasticity, two scenarios may occur: either (i) the maximal instability growth rate exhibits a monotonic dependence on the wave height, or (ii) complete stabilization is achieved for sufficiently large heights within numerical tolerance.

1. Introduction

The Whitham equation first appeared in the literature as a heuristic model with the same degree of nonlinearity as the Korteweg–de Vries (KdV) equation, but with the exact unidirectional dispersion relation of the full water wave problem [1,2]. The motivation behind Whitham's model was to propose a simple yet effective equation capable of capturing short waves, sharp crests, and wave breaking (gradient cathastrofe as in the Burgers equation) phenomena that the KdV equation fails to describe due to its perfect balance between dispersion and nonlinearity. However, if the kinematic (or convective) breaking criterion is used, it has been shown that the maximum wave height for solitary waves is about 0.687, with similar results for cnoidal waves [3,4]. A common criticism is that the KdV equation is valid only for small amplitudes, whereas the breaking threshold concerns moderate amplitudes. This can be countered by noting that the shallow-water system is itself valid only for long waves, while shock formation is a short-wave phenomenon; hence the most common wave-breaking model can be critiqued on the same grounds.

In its simplest form, the Whitham equation is given by

$$u_t + 2uu_x + K * u_x = 0, \tag{1}$$

where K is a nonlocal operator whose Fourier multiplier is defined by

$$\widehat{K}(k) = \sqrt{\frac{\tanh k}{k}}. \tag{2}$$

Although originally introduced in an ad-hoc manner, bidirectional Whitham-type models — known as Whitham-Boussinesq systems — can be derived formally from Hamiltonian principles (see [5–9]). Because of the wide range of nonlinear phenomena it captures, the Whitham equation has become a model of central importance in both applied and pure mathematics. Over the past decade, the equation has been the subject of extensive study. The existence of traveling-wave solutions and the proof of the Whitham conjecture were established in [10–12]. For the capillary–gravity Whitham equation, the existence of solitary-wave solutions was established in the works [13,14]. The existence of asymmetric periodic traveling–wave solutions of arbitrarily small amplitude has also been established; such waves occur only in the weak surface–tension regime [15]. Numerical evidence that all large-amplitude, periodic traveling-wave solutions of the Whitham equation are spectrally unstable for every wavelength was reported in [16], in agreement with theoretical results reported later in [17]. Hur and Johnson showed that all small–amplitude periodic traveling waves are spectrally stable when their wavelength exceeds a critical threshold and unstable below it [17]. The superharmonic instability was discussed recently in the work of Carter [18]. Carter computed 2π-periodic traveling-wave solutions of the Whitham equation and, focusing on large steepness, showed that the Hamiltonian oscillates with steepness for sufficiently steep waves. Numerical studies of spectral stability, including the effects of constant vorticity [19], have reproduced the classical "figure-eight" instability curve associated with modulational instability, also reported within Whitham-Boussinesq systems [20]. The spectral stability of solitary waves in both the Whitham and the capillary–gravity Whitham equations were proved recently [21]. Carter and Rozman analyzed the spectral stability of periodic traveling waves in the capillary–gravity setting . In particular, they computed families of solutions with a single dominant wavenumber and families with multiple dominant wavenumbers, finding that when a single dominant wavenumber is present the maximal instability growth rate increases with the wave height, whereas in the multi-wavenumber case no simple relationship between growth rate and height emerges [22]. Theoretical criteria for modulational instability for a broad class of generalized Whitham equations — allowing for different flux functions and nonlocal operators — were developed in [23]. In particular, an explicit criterion to determine the modulational stability or instability of small-amplitude periodic traveling-wave solutions was provided. Further contributions include studies of solitary-wave collisions and verification of the geometric Lax classification [24,25], as well as investigations of solitary-wave interactions under external forcing [26,27]. Comparisons between the KdV and Whitham models have been carried out both theoretically [28] and numerically [29], including benchmarks against the full Euler equations.

Several extensions of the Whitham equation have appeared in the literature. For instance, and Kharif et al. and Kharif and Abid proposed a heuristic model known as the Cubic Vortical Whitham (CV-Whitham) equation, which serves as an asymptotic approximation (in dispersion) of the Gardner equation to study nonlinear water waves on a vertically sheared current of constant vorticity in shallow water [30,31]. This model preserves the unidirectional linear dispersion relation. Subsequent works addressed the spectral stability of periodic waves [32] and investigated solitary-wave interactions and breather formation [33,34]. In the context of the Cubic Whitham equation, Kalisch et al. provided strong numerical evidence for the existence of breather solutions [35], while Flamarion and Pelinovsky studied overtaking collisions [36] . Another important extension is the hydroelastic Whitham equation, which models wave propagation in a thin elastic sheet overlying an incompressible, inviscid fluid. Dinvay et al. analyzed periodic waves in this setting and compared their bifurcation curves (wave height vs. speed) with those of the full Euler equations [9]. However, the spectral stability of hydroelastic Whitham waves remains an open problem.

The aim of this work is to study the spectral stability of periodic traveling waves of the hydroelastic Whitham equation. Periodic solutions are computed via a Newton-type method, and stability is analyzed by linearizing about the wave and applying the Fourier–Floquet–Hill method [37]. For weak elasticity (gravity-dominated dispersion), the Bloch spectrum exhibits the classical figure-eight instability pattern even at small wave heights H, with a nonmonotonic growth rate that bifurcates into ellipse-like loops, indicating enhanced sideband instabilities. For moderate elasticity, two distinct cases are observed: (i) the waves remain unstable as the height grows, with the compact figure-eight near the origin; or (ii) the waves eventually reach complete stabilization. In the strongly elastic regime, the spectrum lies entirely on the imaginary axis and no figure-eight or loop structures appear, confirming spectral stability.

The remainder of the article is organized as follows: Section 2 introduces the hydroelastic Whitham equation; Section 3 formulates the problem; Section 4 outlines the numerical methods; Section 5 presents the results; and Section 6 offers concluding remarks.

2. The hydroelastic Whitham

We consider the hydroelastic Whitham [9] equation in canonical form

$$u_t + 2u u_x + \mathcal{K} * u_x = 0, \tag{3}$$

where $u = u(x, t)$ denotes the wave field and $*$ is convolution in x. The nonlocal operator $\mathcal{K}$ is the Fourier multiplier with real, even symbol

$$\widehat{\mathcal{K}}(k) = \sqrt{\left(1 + T k^4\right) \frac{\tanh k}{k}}, \tag{4}$$

which incorporates gravity and flexural (elastic) dispersion; here $T \geq 0$ is proportional to the elastic stiffness. The reader may be familiarized with the capillary–gravity Whitham equation which has the form

$$u_t + 2u u_x + \mathcal{K}_{cg} * u_x = 0, \tag{5}$$

where

$$\widehat{\mathcal{K}}_{cg}(k) = \sqrt{\left(1 + T k^2\right) \frac{\tanh k}{k}}, \tag{6}$$

is capillary–gravity correction; surface tension enters as k^2. Before further proceed we highlight the similarities and differences of both equations. For the capillary–gravity Whitham equation the dispersion symbol undergoes a monotonicity transition at the critical value $T_c = 1/3$. When $T = 0$, $\widehat{\mathcal{K}}_{cg}$ is strictly decreasing on $(0, \infty)$ and satisfies $\widehat{\mathcal{K}}_{cg}(k) \to 0$ as $k \to \infty$. For $0 < T < 1/3$, $\widehat{\mathcal{K}}_{cg}$ is non–monotone: it decreases for small k and increases for large k, possessing a unique local minimum at some $k^*(T) \in (0, \infty)$. For $T \geq 1/3$, $\widehat{\mathcal{K}}_{cg}$ is monotone increasing on $(0, \infty)$; in particular, at $T = 1/3$ it is flat to order k^2 at $k = 0$ and then increases.

By contrast, for the hydroelastic (k^4) model with symbol

$$\widehat{\mathcal{K}}(k) = \sqrt{(1 + Tk^4)\frac{\tanh k}{k}}, \tag{7}$$

the small–k expansion reads

$$\widehat{\mathcal{K}}(k) = 1 - \frac{k^2}{6} + \left(\frac{19}{360} + \frac{T}{2}\right)k^4 + O(k^6). \tag{8}$$

The k^2–coefficient is independent of T (as in pure gravity), so the phase speed is initially decreasing. On the other hand, as $k \to \infty$ we have $\widehat{\mathcal{K}}(k) \sim \sqrt{T} k^{3/2}$, hence it ultimately increases. Therefore, for every $T > 0$ the hydroelastic symbol is non–monotone and attains a local minimum at some $k^*(T) > 0$. Consequently, waves of different wavelengths can travel at the same phase speed, and one should expect qualitative features analogous to the capillary–gravity case with $0 < T < 1/3$ (e.g., bimodal interactions and non–monotone wave profiles).

The spectral stability of periodic waves within capillary–gravity waves was investigated within different wavenumbers in [22]. For 2π–periodic waves, the authors showed that at such waves are modulational unstable for $T \geq 1/3$. For $0 < T < 1/3$, the authors were unable to compute 2π–periodic waves.

3. Mathematical formulation

We are interested in the spectral stability of 2π-periodic traveling waves of the Whitham equation, we begin by constructing such waves and then linearizing the dynamics about the resulting periodic profile. This method has been described in detail by Sanford et al. [16], but for the sake of self-containment we briefly recall the main steps and fix notation.

We seek 2π-periodic traveling waves of speed c in the form

$$u(x,t) = f(z), \qquad z = x - ct. \tag{9}$$

Substituting into (3) and writing derivatives with respect to z gives

$$-c f' + 2f f' + (\mathcal{K} * f') = 0. \tag{10}$$

Using that convolution commutes with differentiation, $\mathcal{K} * f' = \partial_z(\mathcal{K} * f)$, we integrate (10) once in z to obtain

$$-c f + f^2 + \mathcal{K} * f = 0. \tag{11}$$

Here, we follow [16] and set the integration constant in (11) to zero. The numerical method to obtain $f(z)$ is described in the following section.

To analyze spectral stability, we perturb the traveling wave by a small disturbance and linearize:

$$u(x,t) = f(z) + \epsilon w(z,t), \qquad 0 < \epsilon \ll 1, \quad z = x - ct. \tag{12}$$

Substituting (12) into the PDE and collecting $\mathcal{O}(\epsilon)$ terms yields, in the moving coordinate z,

$$w_t - c w_z + 2(f w)_z + \mathcal{K} * w_z = 0. \tag{13}$$

Using $\mathcal{K} * w_z = \partial_z(\mathcal{K} * w)$, we can write (13) in conservative form

$$w_t = -2f'w + (c - 2f)w_z - \mathcal{K} * w_z =: \mathcal{L}w, \tag{14}$$

with 2π-periodic f and convolution operator $\mathcal{K}$. Introduce

$$f_0(z) := -2f'(z), \qquad f_1(z) := c - 2f(z), \tag{15}$$

therefore

$$w_t = f_0(z) w + f_1(z) w_z - \mathcal{K} * w_z =: \mathcal{L}w. \tag{16}$$

Bloch–Floquet decomposition. Because f is 2π-periodic, we decompose perturbations into Bloch waves. For $\xi \in [-\frac{1}{2}, \frac{1}{2}]$, seek

$$w(z,t) = e^{\lambda t} e^{i\xi z} \phi(z), \qquad \phi(z + 2\pi) = \phi(z). \tag{17}$$

Let $(\partial_z + i\xi)$ denote the Bloch derivative and let $\mathcal{K}_\xi$ be the shifted multiplier defined by

$$\widehat{(\mathcal{K}_\xi \phi)}(k) = \widehat{\mathcal{K}}(k + \xi)\widehat{\phi}(k), \qquad k \in \mathbb{Z}.$$

Inserting (17) into (16) gives the family of eigenvalue problems

$$\lambda\phi = f_0\,\phi \;+\; \left(f_1 - \mathcal{K}_\xi\right)(\partial_z + i\xi)\phi = (\partial_z + i\xi)\Big[f_1\,\phi - \mathcal{K}_\xi\phi\Big] = \mathcal{L}\phi, \tag{18}$$

where the two expressions are equivalent since $\mathcal{K}_\xi$ and $(\partial_z + i\xi)$ commute. The spectrum of the linearized operator is

$$\sigma_{\text{spec}} = \bigcup_{\xi\in[-\frac{1}{2},\frac{1}{2}]} \sigma(\mathcal{L}_\xi), \qquad \mathcal{L}_\xi := f_0 + \left(f_1 - \mathcal{K}_\xi\right)(\partial_z + i\xi). \tag{19}$$

Spectral stability holds if $\Re\lambda \le 0$ for all $\lambda \in \sigma_{\text{spec}}$ while instability is detected when $\Re\lambda > 0$.

4. Numerical methods

We compute 2π-periodic traveling-wave solutions with height H and phase speed c using Newton's method, following [25,33]. This is accomplished by solving

$$-cu_x + 2uu_x + \mathcal{K} * u_x = 0,$$
$$u(0) - u(\pi) - H = 0. \tag{20}$$

Eq. (20) can be written in Fourier space as

$$-c\widehat{u} + \widehat{u^2} + \widehat{\mathcal{K}}\widehat{u} = 0,$$
$$u(0) - u(\pi) - H = 0. \tag{21}$$

We consider N points uniformly space in the computational domain $[-\pi, \pi]$, namely,

$$x_j = -\pi + j\Delta x, \;\; j = 0, 1, \dots, N-1, \text{ where } \Delta x = 2\pi/N. \tag{22}$$

Denoting by $u_j = u(x_j)$ for $j = 0, 1, 2, \dots, N-1$, the discretized version of u is the vector

$$\mathbf{u} = (u_0, u_2, \dots, u_{N-1}). \tag{23}$$

Substituting (23) into Eq. (21), we obtain the discretized system of equations

$$-c\mathbf{F}[\mathbf{u}] + \mathbf{F}[\mathbf{u}^2] + \mathbf{F}[\mathcal{K}]\mathbf{F}[\mathbf{u}] = 0,$$
$$\mathbf{u}_{N/2+1} - u_0 - H = 0. \tag{24}$$

Here, $\mathbf{F}[u] = (\mathbf{F}_{k_0}[u], \mathbf{F}_{k_1}[u], \dots, \mathbf{F}_{k_{N-1}}[u])$ represents the discrete Fourier transform, with components given by

$$\mathbf{F}_{k_n}[u] = \sum_{j=0}^{N-1} u_j e^{-2\pi i \frac{k_n}{N} j}, \quad n = 0, 1, \dots, N-1, \tag{25}$$

where the corresponding frequencies are defined as

$$(k_0, k_1, \dots, k_{N-1}) = (0, 1, \dots, N-1). \tag{26}$$

Solutions to the system of Eqs. (24) are computed by finding the zeros of $\mathcal{G} : \mathbb{R}^{N+1} \to \mathbb{R}^{N+1}$ defined as

$$\mathcal{G}(u_0, u_1, \dots, u_{N-1}, c) = (G_0, G_1, \dots, G_N), \tag{27}$$

where

$$G_j(u_0, u_1, \dots, u_{N-1}, c) := -c\mathbf{F}[\mathbf{u}] + \mathbf{F}[\mathbf{u}^2] + \mathbf{F}[\mathcal{K}]\mathbf{F}[\mathbf{u}] = 0, \text{ for } j = 1, 2, \dots, N,$$
$$G_{N+1}(u_1, u_2, \dots, u_N, c) := u_{N/2+1} - u_0 - H = 0. \tag{28}$$

The Jacobian for Newton's method is computed using finite differences with respect to the unknown variables, specifically,

$$\frac{\partial G_n}{\partial u_j} \approx \frac{G_n(u_0, u_1, \dots, u_j + \delta, \dots, u_{N-1}, c) - G_n(u_0, u_1, \dots, u_j, \dots, u_{N-1}, c)}{\delta}, \text{ for } j = 0, 1, \dots, N-1$$

and

$$\frac{\partial G_n}{\partial c} \approx \frac{G_n(u_0, u_1, \dots, u_j, \dots, u_{N-1}, c + \delta) - G_n(u_0, u_1, \dots, u_j, \dots, u_{N-1}, c)}{\delta},$$

for $n = 0, 1, \dots, N$ and $\delta = 10^{-10}$. The stopping criterion adopted is

$$\frac{\sum_{j=1}^{N+1} |G_n(u_1, u_2, \dots, u_{N-1}, c)|}{N+1} < \epsilon,$$

where ϵ is a given tolerance, which we choose $\epsilon = 10^{-12}$.
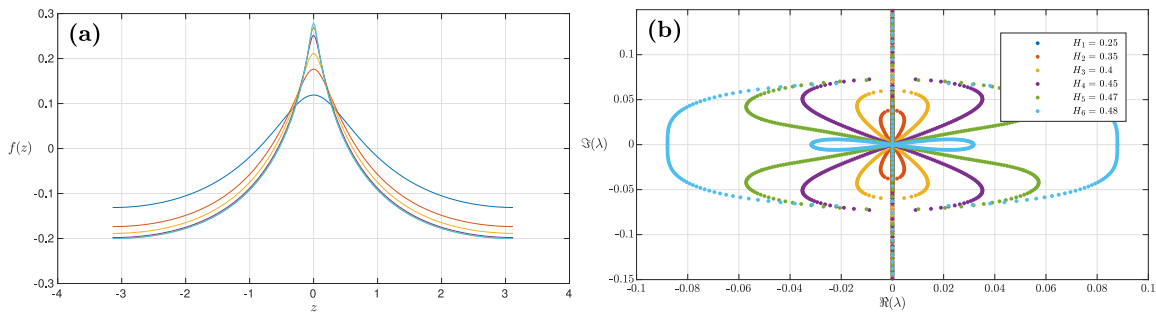
Fig. 1. (a) Periodic traveling waves with different heights and the corresponding spectrum (b) for $T = 0$.

The discrete Fourier transforms in system (28) are efficiently computed using the Fast Fourier Transform (FFT) algorithm [38]. It is important to note that the solution obtained is in Fourier space; however, the physical-space solution can be recovered by applying the inverse Fourier transform as

$$u_j = \frac{1}{N} \sum_{n=0}^{N-1} \mathbf{F}_{k_n}[\mathbf{u}] e^{2\pi i \frac{k_n}{N} j} \text{ for } j = 0, 1, \dots, N - 1. \tag{29}$$

The Newton method is initiated with the initial guess (u_0, c_0), where

$$u_0(x) = \epsilon_0 \cos(k_0 x), \text{ and } c_0 = \sqrt{(1 + T k_0^4) \frac{\tanh(k_0)}{k_0}}; \tag{30}$$

where ϵ_0 is the initial wave amplitude and k_0 is the wave number.

The operator (18) is discretized in a infinity matrix as in [16,37]

$$\widehat{\mathcal{L}}_{nm}(\mu) = \begin{cases} \widehat{f_0}(n-m) + i(\mu + m)\widehat{f_1}(n-m), & m \neq n, \\ \widehat{f_0}(0) + i(\mu + n)\widehat{f_1}(0) - i(\mu + n)\mathcal{K}(\mu + n), & m = n, \end{cases} \quad n, m \in \mathbb{Z}, \tag{31}$$

where f_0 and f_1 are defined in Eq. (15). and the hydroelastic Whitham symbol is

$$\mathcal{K}(s) = \sqrt{\left(1 + T s^4\right) \frac{\tanh s}{s}}, \qquad s \in \mathbb{R}. \tag{32}$$

In the computations reported in the next section, we use $N = 2^9$ Fourier modes. Grid independence is confirmed by repeating the simulations with $N = 2^8$ and $N = 2^{10}$; the results are indistinguishable, indicating independence from the grid resolution.

5. Results

We investigate the spectral stability of hydroelastic waves for a range of values of T. We are particularly interested in the effect of elastic stiffness on the spectral stability of 2π-periodic waves. Unlike the capillary–gravity Whitham equation—where one typically contrasts the regimes $T < 1/3$, $T = 1/3$ and $T > 1/3$ due to the qualitative change in the linear symbol at $T = 1/3$. Since no such bifurcation occurs for the hydroelastic symbol, we assess the effect of the elasticity coefficient T on the stability of 2π-periodic waves by classifying T according to its magnitude at the fundamental mode $k = 1$, consistent with our focus on 2π-periodic solutions. Specifically, we focus on three representative cases: (i) $T = 0.01$ (small stiffness), (ii) $T = 0.1$ and $T = 0.45$ (moderate stiffness), and (iii) $T = 10$ (strong stiffness). For completeness, additional cases are discussed at the end of this section.

As a benchmark, we first set $T = 0$ (absence of the elastic sheet), recovering the classical gravity Whitham equation. Fig. 1 shows a family of 2π-periodic traveling waves with varying height H (crest–trough amplitude). For small heights, the spectrum of the linearization about the wave lies on the imaginary axis, indicating spectral stability. As the height increases past $H \approx 0.30$, a collision at the origin generates the classical figure-eight pattern in the Bloch spectrum, signaling the onset of a modulational (Benjamin–Feir type) instability. This figure-eight persists as H grows and, near $H \approx 0.47$, undergoes a secondary reorganization: the loop reorients into a "horizontal" figure-eight, which then bifurcates further into a detached, ellipse-like loop off the imaginary axis (see Fig. 1). These features are consistent with previously reported spectral portraits for the Whitham equation and corroborate earlier computations in the literature, see for instance [16], thereby validating our numerical implementation.

Next, we increase the elasticity slightly to $T = 0.01$, so the model describes hydroelastic waves. Along the 2π-periodic branch, as the wave height increases, single-crested profiles undergo a transition to four-crested periodic waves (Fig. 2(a)), indicating that elastic effects in this parameter regime. This is similar to what is observed for capillary–gravity waves when $T < 1/3$, where ripples appear on the traveling wave. The corresponding Bloch spectra are shown in Fig. 2(b). Compared with the gravity-only case ($T = 0$), the spectral picture changes qualitatively: the figure-eight loop that signals modulational instability first expands with the
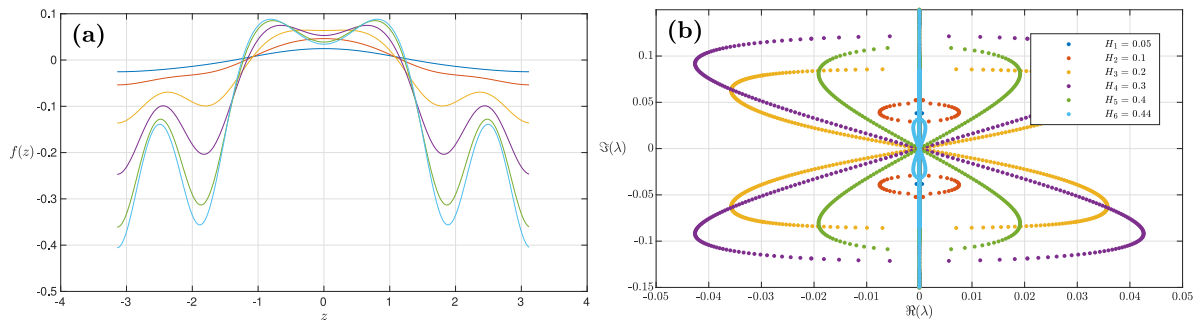
Fig. 2. (a) Periodic traveling waves with different heights and the corresponding spectrum (b) for $T = 0.01$.
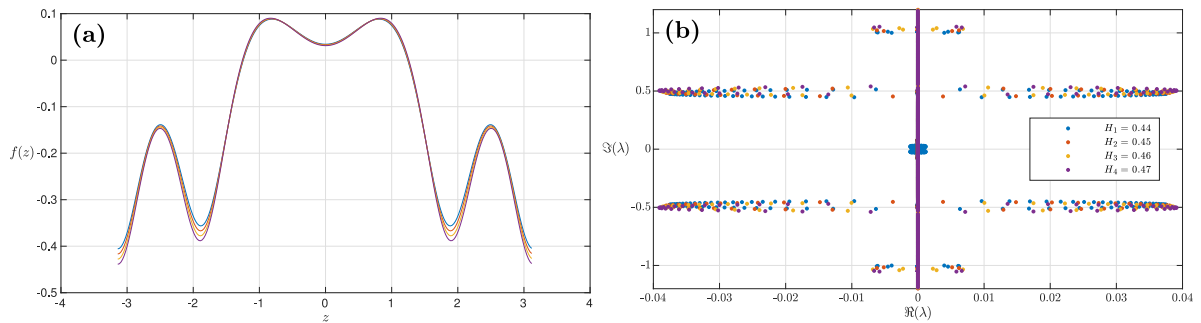

Fig. 3. (a) Periodic traveling waves with different heights and the corresponding spectrum (b) for $T = 0.01$.

wave height H up to a critical amplitude $H = H_c$, and then contracts back toward the imaginary axis. Consequently, the maximal growth rate

$$\max_{\xi \in [-\frac{1}{2}, \frac{1}{2}]} \max \Re \sigma(L_\xi) \tag{33}$$

is non-monotone in H, and sufficiently large-height periodic waves on this branch reach stabilization, but not complete. This stabilization at large height is consistent with previous observations for related Whitham-type models, where added short-wave dispersion can reverse the modulational (Benjamin–Feir) index at finite height; see, for instance, Fig. 9, for gravity–capillary Whitham waves [22]. Although stabilization occurs, it is not complete: the spectrum undergoes a secondary bifurcation in which the horizontal figure-eight splits into a sequence of ellipse-like loops, symmetric about — and centered on — the imaginary axis; see Fig. 3 for details. In our setting, the elastic term (controlled by T) enhances high-wavenumber dispersion, which deforms the figure-eight loop, delays the onset of sideband growth. We also note that the rapid emergence of four-crested profiles from the single-crested branch is suggestive of a subharmonic (1:4) resonance, though a full bifurcation classification is beyond our present scope. For a comprehensive bifurcation classification of the hydroelastic Whitham equation—see [9] and also [39] for capillary–gravity waves.

For moderate elasticity ($T = 0.1$), our computations show that even small-amplitude 2π-periodic waves are spectrally unstable (see Fig. 4). At small height H, the Bloch spectrum exhibits a compact figure-eight near the origin; as H increases, this loop rotates into a horizontal figure-eight. The corresponding spectral growth rate (i.e., the maximal real part of the spectrum) increases up to a certain amplitude and then decreases, as illustrated in Fig. 4. Crucially, the behavior at larger amplitudes differs from the $T = 0.01$ case: instead of the spectrum undergoes a secondary bifurcation in which the horizontal figure-eight breaks into a sequence of ellipse-like loops symmetric about (and with centers on) the imaginary axis it reaches complete stabilization. It is worth noting that, for the gravity Whitham equation, the maximal instability growth rate increases with wave height. For the capillary–gravity Whitham equation, Carter and Rozman likewise reported that, when solutions exhibit a single dominant wavenumber, the maximal growth rate increases with wave height [22]. In contrast, our results differ qualitatively: because we restrict attention the maximal instability growth rate does not increase as H increases. Fig. 5 demonstrates the complete stabilization of the spectrum for 2π-periodic waves across a range of amplitudes (within numerical tolerance). Note that in Fig. 5 the x-axis is scaled by 10^{-8}.

Still within the regime of moderate elasticity, but considering the case $T = 0.45$, a qualitatively different behavior is uncovered. Unlike the case $T = 0.1$, where instability persists even for small amplitudes, the 2π-periodic waves of small height remain spectrally stable. As the wave height increases, however, these solutions undergo a transition to modulational instability, with the maximal growth rate increasing monotonically with H. This regime thus represents an intermediate transition between the weakly elastic and fully stabilized cases. Fig. 6 illustrates several representative traveling-wave profiles together with their corresponding Bloch spectra, highlighting the emergence and subsequent strengthening of the unstable sideband modes as H increases.
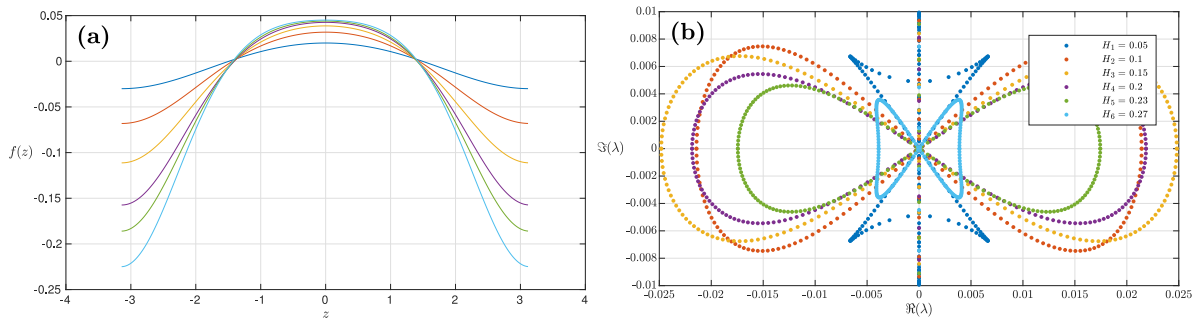
Fig. 4. (a) Periodic traveling waves with different heights and the corresponding spectrum (b) for $T = 0.1$.
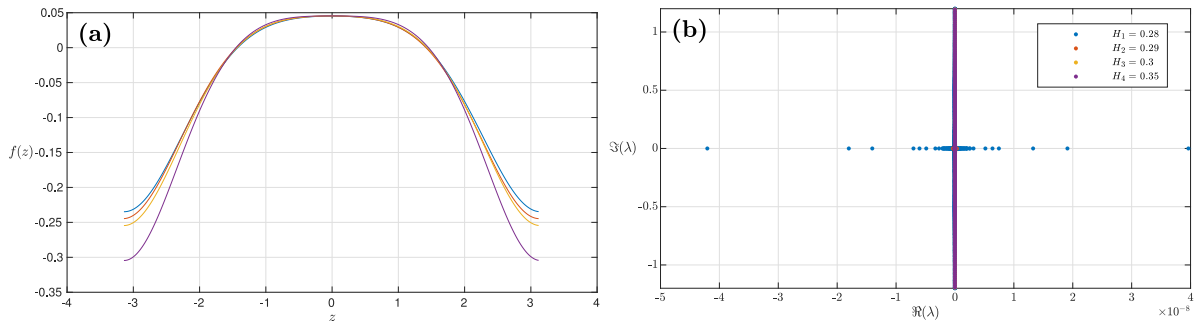

Fig. 5. (a) Periodic traveling waves with different heights and the corresponding spectrum (b) for $T = 0.1$.
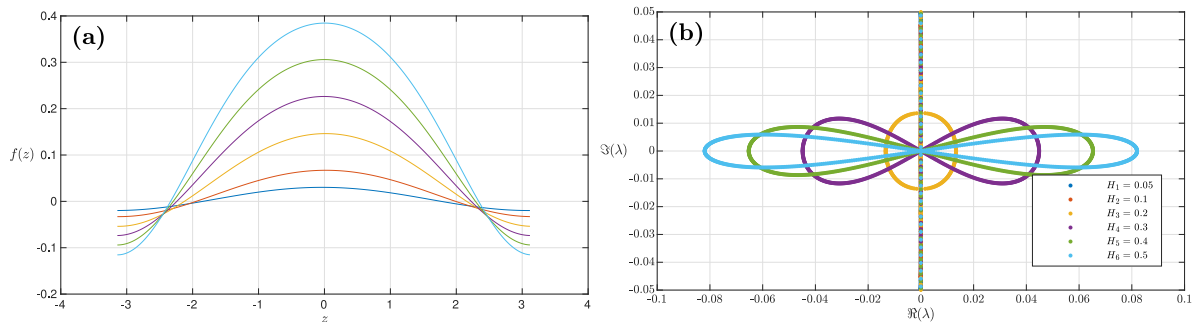

Fig. 6. (a) Periodic traveling waves with different heights and the corresponding spectrum (b) for $T = 0.45$.

For strongly elastic regime ($T = 10$), long the entire 2π-periodic branch computed, the Bloch spectra remain confined to the imaginary axis (within numerical tolerance), and no figure-eight or ellipse-type loops form, see Fig. 7. Hence, all periodic waves in this regime are spectrally stable. From a dispersion standpoint, large T amplifies the high-wavenumber part of the symbol

$$\widehat{\mathcal{K}}(k) = \sqrt{(1 + Tk^4)\frac{\tanh k}{k}}, \tag{34}$$

so that $\widehat{\mathcal{K}}(k) \sim \sqrt{T}\,k^2\sqrt{\tanh k/k}$; in particular, for small k one has $\widehat{\mathcal{K}}(k) \approx \sqrt{T}\,k^2$. This enhanced dispersive effect counteracts the nonlinear steepening responsible for modulational (Benjamin–Feir) instabilities, preventing the eigenvalue collisions that generate figure-eight structures and thereby stabilizing the periodic waves across the amplitudes investigated. Another way to see this is by noticing that in the large-T regime the hydroelastic Whitham equation is asymptotically close (in the long-wave/small-amplitude limit) to the KdV model. For KdV, all periodic traveling-wave (cnoidal) solutions are spectrally stable; see [40].

To summarize our findings, Fig. 8 plots the maximal growth rate (the real part of the most unstable eigenvalue) as a function of the 2π-periodic wave height H for several values of the elasticity parameter T. The curves are obtained from a series of simulations with grid-refinement checks. For $T = 0$, the maximal growth rate increases monotonically with the wave height H, indicating a continuous amplification of modulational instability as the amplitude grows. As the flexural rigidity coefficient T increases, distinct
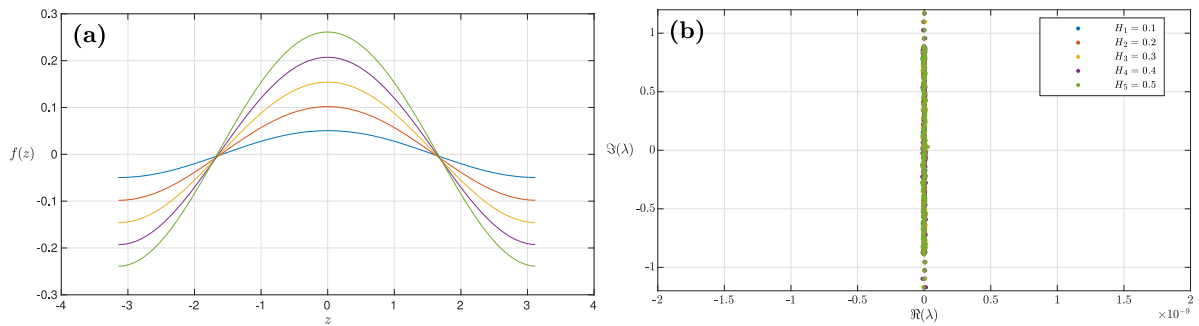
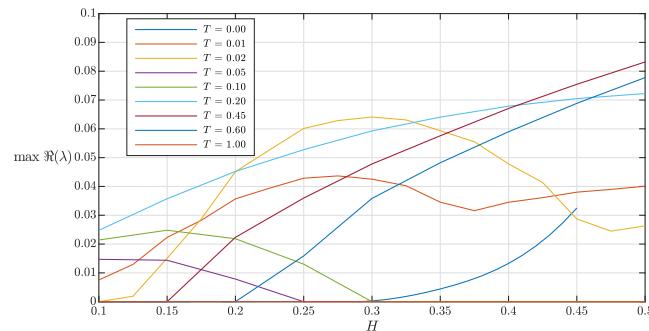**Fig. 7.** (a) Periodic traveling waves with different heights and the corresponding spectrum (b) for $T = 10$.

Fig. 8. The maximal growth rate (the real part of the most unstable eigenvalue) as a function of the 2π-periodic wave height H for different values of T.

stability regimes emerge. For weak elasticity ($0.01 \leq T < 0.05$), the dependence of the maximal growth rate on H becomes distinctly oscillatory, reflecting the onset of complex sideband interactions at small T. In the regime of moderate elasticity ($0.05 \leq T \leq 0.10$), the maximal growth rate exhibits a nonmonotonic dependence on H, eventually leading to stabilization at larger amplitudes. A monotonic increase of the maximal growth rate with respect to H is observed for $0.1 < T \leq 0.7$, indicating a progressive amplification of modulational instability as T grows. When $T > 0.7$, all 2π-periodic wave solutions are found to be spectrally stable within numerical accuracy, and complete stabilization is achieved.

6. Conclusions

We have numerically investigated the spectral stability of 2π-periodic traveling waves for the hydroelastic Whitham equation across a range of elasticity parameters $T \geq 0$. The spectra were computed by a Bloch–Floquet (Hill) approach with Fourier collocation, applying the nonlocal dispersion through its Fourier multiplier and assembling the spectra of the Bloch operators. For weak elasticity (gravity-dominated dispersion), the Bloch spectrum exhibits the classical figure-eight pattern even for relatively small wave heights H, signaling modulational (Benjamin–Feir) instability; moreover, the associated growth rate is non-monotone in H, with the loop expanding up to a critical amplitude and then shrinking, however, instead of reaching complete stabilization, the pattern undergoes a secondary reorganization, rotating into a horizontal figure-eight configuration that may further bifurcate into one or more ellipse-like loops centered along the imaginary axis, indicating enhanced sideband instabilities at higher amplitudes. For moderate elasticity, where gravitational and elastic effects are comparable, two distinct scenarios may arise: (i) the maximal instability growth rate displays a monotonic dependence on the wave height, or (ii) complete stabilization occurs at sufficiently large amplitudes within numerical tolerance. When elasticity dominates, the spectra along the entire branch remain confined to the imaginary axis within numerical tolerance; no figure-eight or ellipse-type loops are observed and the waves are spectrally stable. These findings are consistent with the enhanced high-wavenumber dispersion introduced by the elastic term, which counteracts nonlinear steepening and prevents the eigenvalue collisions that trigger modulational instability.

CRediT authorship contribution statement

Marcelo V. Flamarion: Writing – review & editing, Writing – original draft, Methodology, Investigation, Formal analysis, Conceptualization. **Jimmie Adriazola:** Writing – review & editing, Methodology, Investigation, Formal analysis, Conceptualization.

Declaration of competing interest

The authors declare that they have no known competing financial interests or personal relationships that could have appeared to influence the work reported in this paper.

Acknowledgments

Data availability

Data sharing is not applicable to this article as all parameters used in the numerical experiments are informed in this paper.

References

[1] G.B. Whitham, Linear and Nonlinear Waves, John Wiley & Sons, Inc, New York, 1974.
[2] G.B. Whitham, Variational methods and applications to water waves, Proc. R. Soc. Lond. A 229 (1967) 6–25.
[3] M.K. Brun, H. Kalisch, Convective wave breaking in the KdV equation, Anal. Math. Phys. 8 (1) (2018) 57–75.
[4] A. Senthilkumar, H. Kalisch, Wave breaking in the KdV equation on a flow with constant vorticity, Eur. J. Mech. B Fluids 73 (2019) 48–54.
[5] J.D. Carter, Bidirectional Whitham equations as models of waves on shallow water, Wave Motion 82 (2018) 51–61.
[6] E. Dinvay, D. Dutykh, H. Kalisch, A comparative study of bi-directional Whitham systems, Appl. Numer. Math. 141 (2019) 248–262.
[7] R.M. Vargas-Magaña, T.R. Marchant, N. Smyth, Numerical and analytical study of undular bores governed by the full water wave equations and bidirectional Whitham-Boussinesq equations, Phys. Fluids 33 (2021) 067105.
[8] C. Yuan, Z. Wang, Bidirectional Whitham type equations for internal waves with variable topography, Ocean Eng. 257 (2022) 111600.
[9] E. Dinvay, H. Kalisch, D. Moldabayev, E.I. Părău, The Whitham equation for hydroelastic waves, Appl. Ocean Res. 89 (2019) 202–210.
[10] M. Ehrnström, H. Kalisch, Traveling waves for the Whitham equation, Differ. Integral Equ. Appl. 22 (2009) 1193–1210.
[11] M. Ehrnström, M.D. Groves, E. Wahlén, On the existence and stability of solitary-wave solutions to a class of evolution equations of Whitham type, Nonlinearity 25 (10) (2012) 2903.
[12] M. Ehrnström, E. Wahlén, On Whitham's conjecture of a highest cusped wave for a nonlocal dispersive equation, Ann. I. H. Poincare-An 36 (2019) 769–799.
[13] M. Arnesen, Existence of solitary-wave solutions to nonlocal equations, Discrete Contin. Dyn. Syst. 36 (2016) 3483–3510.
[14] M.A. Johnson, T. Truong, M.H. Wheeler, Solitary waves in a Whitham equation with small surface tension, Stud. Appl. Math. (2021).
[15] O. Mæhlen, D. Svensson Seth, Asymmetric Traveling Wave Solutions of the Capillary–Gravity Whitham Equation, SIAM J. Math. Anal. 56 (6) (2024) 8096–8124.
[16] N. Sanford, K. Kodama, J.D. Carter, H. Kalisch, Stability of traveling wave solutions to the Whitham equation, Phys. Lett. A 378 (30–31) (2014) 2100–2107.
[17] V.M. Hur, M. Johnson, Modulational instability in the Whitham equation for water waves, Stud. Appl. Math. 134 (2015) 120–143.
[18] J.D. Carter, Instability of near-extreme solutions to the Whitham equation, Stud. Appl. Math. 152 (2024) 903–915.
[19] C. Kharif, M. Abid, J.D. Carter, H. Kalisch, Stability of periodic progressive gravity wave solutions of the Whitham equation in the presence of vorticity, Phys. Lett. A 384 (2) (2020) 126060.
[20] B. Deconinck, O. Trichtchenko, High-frequency instabilities of small-amplitude Hamiltonian PDEs, Discrete Contin. Dyn. Syst. 37 (3) (2015) 1323–1358.
[21] M. Cadiot, Constructive proofs of existence and stability of solitary waves in the Whitham and capillary–gravity Whitham equations, Nonlinearity 38 (2025) 035021.
[22] J.D. Carter, M. Rozman, Stability of periodic, traveling-wave solutions to the capillary Whitham equation, Fluids 4 (58) (2019).
[23] A.L. Binswanger, M.A. Hoefer, B. Ilan, P. Sprenger, Whitham modulation theory for generalized Whitham equations and a general criterion for modulational instability, Stud. Appl. Math. 147 (2021) 724–751.
[24] P.D. Lax, Integrals of nonlinear equations of evolution and solitary waves, Commun. Pure Appl. Math. 21 (1968) 467–490.
[25] M.V. Flamarion, Solitary wave collision for the Whitham equation, Comp. Appl. Math. 41 (356) (2022).
[26] M.V. Flamarion, Trapped waves generated by an accelerated moving disturbance for the Whitham equation, Partial. Differ. Equ. Appl. Math. 5 (2022) 100356.
[27] M.V. Flamarion, Waves generated by a submerged topography for the Whitham equation, Int. J. Appl. Comput. Math. 8 (257) (2022).
[28] C. Klein, F. Linares, D. Pilod, J.C. Saut, On Whitham and related equations, Stud. Appl. Math. 140 (2018) 133–177.
[29] D. Moldabayev, H. Kalisch, D. Dutykh, The Whitham equation as a model for surface water waves, Physica D 309 (2015) 99–107.
[30] C. Kharif, M. Abid, J. Touboul, Rogue waves in shallow water in the presence of a vertically sheared current, J. Ocean. Eng. Mar. Energy 3 (2017) 301–308.
[31] C. Kharif, M. Abid, Nonlinear water waves in shallow water in the presence of constant vorticity: A Whitham approach, Eur. J. Mech. B Fluids 72 (2018) 12–22.
[32] J.D. Carter, H. Kalisch, C. Kharif, M. Abid, The cubic vortical Whitham equation, Wave Motion 110 (2022) 102883.
[33] M.V. Flamarion, E. Pelinovsky, Features of the interaction of paired solitary waves with the cubic vortical Whitham equation, Appl. Math. Comput. 493 (2025) 129265.
[34] M.V. Flamarion, E. Pelinovsky, Wave evolution within the cubic vortical Whitham equation, Wave Motion 134 (10348) (2025).
[35] H. Kalisch, M.A. Alejo, A.J. Corcho, D. Pilod, Breather solutions to the cubic Whitham equation, 2022, arXiv:2201.12074v2.
[36] M.V. Flamarion, E. Pelinovsky, Solitary wave interactions in the cubic Whitham equation, Russ. J. Math. Phys. 31 (2) (2024) 199–208.
[37] B. Deconinck, J. Kutz, Computing spectra of linear operators using Hill's method, J. Comput. Phys. 219 (2006) 296–321.
[38] L.N. Trefethen, Spectral Methods in MATLAB, SIAM, Philadelphia, 2001.
[39] E.G. Charalampidis, V.M. Hur, Numerical bifurcation and stability for the capillary–gravity Whitham equation, Wave Motion 106 (2021) 102793.
[40] N. Bottman, B. Deconinck, KdV cnoidal waves are spectrally stable, Discrete Contin. Dyn. Syst. 25 (4) (2009) 1163–1180.